Case Studies in Thermal Engineering 42 (2023) 102716

Contents lists available at ScienceDirect

Case Studies in Thermal Engineering

journal homepage: www.elsevier.com/locate/csite

Effect of surfactants on the convective heat transfer and pressure drop characteristics of ZnO/DIW nanofluids: An experimental study

Adnan Qamar [a], Rabia Shaukat [a], Shahid Imran [a], Muhammad Farooq [a], Muhammad Amjad [a], Zahid Anwar [a], Hassan Ali [b], Muhammad Farhan [a,**], M.A. Mujtaba [a], Theodosios Korakianitis [c], M.A. Kalam [d], Fares Almomani [e,*]

[a] Department of Mechanical, Mechatronics and Manufacturing Engineering, New-Campus, University of Engineering and Technology, Lahore, Pakistan
[b] De Montfort University Leicester, United Kingdom, Dubai Campus, Dubai International Academic City, Post Box: 294345, Dubai, United Arab Emirates
[c] Parks College of Engineering, Aviation and Technology, Saint Louis University, 3450 Lindell Blvd, Saint Louis, MO, 63103, United States
[d] School of Civil and Environmental Engineering, Faculty of Engineering and Information Technology, University of Technology, Sydney, NSW, Australia
[e] Department of Chemical Engineering, College of Engineering, Qatar University, Doha, Qatar

ARTICLE INFO

Handling Editor: Huihe Qiu

Keywords:
Friction factor
Pressure drop
Heat transfer coefficient
Mini tube
Nanofluids
Nanoparticles
Reynolds number
Dispersion stability
Stabilising agents

ABSTRACT

The advancement of nanotechnology has demonstrated the ability of metal-oxide-based nanofluids (NFs) to produce high heat flux in microscale thermal applications. Convective heat transfer (HTC) and flow characteristics (pressure drop (ΔP) and friction factor (*f*)) of aqueous ZnO NFs' within a circular mini tube ($D_i = 1.0$ mm, $L = 330$ mm) were analyzed. Experiments were carried out under steady-state and varying flow rates using 0.012–0.048 wt % of NFs and sodium hexametaphosphate (SHMP) and acetylacetone (ACAC) as surfactants (SFs). Laminar flow and constant wall heat flux conditions were used to assess NFs heat transfer properties, ΔP and *f*. The viscosity (VC) and thermal conductivity (TC) of NFs exhibited a strong dependence on the operating temperature and NFs concentration. VC and TC increased by increasing the NFs concentration and decreased by increasing the operating temperature. Maximum VC and TC enhancement of 16.75% and 23.70% were achieved for SHMP-stabilised NFs, respectively. The average HTC increased by increasing NFs loading and flow rate, with HTC_{max} of 17.0% noticed for ACAC-stabilised NFs. The ΔP_{max} and f_{max} were 16.0% and 12.0%, respectively. Experimental and theoretical results showed a maximum deviation of ±7.0% and ±4.0%, respectively.

1. Introduction

Dissipation of high heat flux is the main challenge in the present era to cope with the cooling requirements of many high-tech modern electronic systems. Despite significant development and research, cooling these systems with reasonable efficacy is still challenging. It led the thermal engineers to develop new methods, techniques, and strategies to overcome this issue [1]. Various

* Corresponding author. Department of Chemical Engineering, College of Engineering, Qatar University, Doha, Qatar.
** Corresponding author. Department of Mechanical, Mechatronics and Manufacturing Engineering, New-Campus, UET, Lahore, Pakistan.
E-mail addresses: m.farhan@uet.edu.pk (M. Farhan), falmomani@qu.edu.qa (F. Almomani).

https://doi.org/10.1016/j.csite.2023.102716
Received 16 November 2022; Received in revised form 3 January 2023; Accepted 6 January 2023
Available online 9 January 2023

techniques, such as enhancing contact surface area, fluid flow rates, induced vibrations, and manipulating conventional fluids' transport properties, are proposed in the literature [2]. However, traditional cooling agents such as distilled water (DW), deionised water (DIW), ethylene glycol (EG), transformer oil, and engine oil possess limited thermophysical and heat transfer characteristics in this regard, and new approaches and cooling agents are highly desired for heat dissipation [3]. A new class of efficient coolants integrated with compact heat exchanging systems is an alternative to dissipating high heat flux from these mini high-tech machines. It will not only shrink the system's size and quantity of fluid but will also improve the thermal systems' heat transfer efficacy with minimal energy consumption. The research community is working extensively for decades in this area to cope with the aforementioned issues.

The thermal performance of traditional heat transfer fluids (HTFs) can be enhanced by adding ultra-fine, small-sized metallic and non-metallic solid particles having high thermal conductivity [4]. The research on this novel concept led thermal engineers to innovate new HTFs, famously known as nanofluids (NFs), containing 1–100 nm particles within volume concentrations up to 5.0%. These small-sized particles dispersed in heat transfer base fluids (BFs) are most commonly known as nanoparticles (NPs) and mainly consist of metallic and non-metallic (metal-oxides) particles. Improved thermophysical properties (thermal conductivity, Brownian motion, etc.) of NFs are supposed to enhance their heat-carrying capability [5]. These NFs will likely enhance the aforementioned modern systems' local and average heat transfer performance. The overall thermal efficiency of any heat transfer system depends upon the effectiveness heat exchanger [6]. The enhanced surface area of the heat-exchanging system plays a key role in increasing the thermal effectiveness of the system. Compact heat exchangers are becoming popular with the advancement in design and shrinking heat exchanging systems because of their reduced size, lesser weight, and increased thermal performance in many applications. Integrating such heat exchanging systems with NFs makes them suitable to cope with high heat flux from the miniature devices [7]. The use of NFs in compact heat exchangers appears promising, but the field faces different challenges in rapid advancement. It includes expensive methods for formulating NFs, poor dispersion stability and heat transfer characteristics of NFs, disagreement between research investigations from various groups, and the absence of helpful information about different mechanisms responsible for heat transfer intensification. The increased pumping power due to increased pressure gradient across the flow channels and collaging of NPs within the minichannel heat exchanging systems is another neglected area [8]. Hence, more in-depth experimental studies are the need of the day to fully recognise these novel fluids' thermal performance and hydraulic characteristics in the microscale heat transfer systems.

1.1. Stability of nanofluids

The dispersion stability of aqueous metal oxide-based NFs is a great challenge for the research community of their potential use in different thermal and heat transfer applications. The sedimentation of the NPs within the host BFs over time makes them unsuitable for their use in compact-sized heat-exchanging systems due to possible blocking and clogging of the tubes and flow channels [9]. Scientists in this field continually explore new horizons and have applied numerous techniques to overcome this issue [10]. Suganthi and Rajan [11] reported the findings for SHMP-stabilised NFs at various SFs and NPs ratios. However, at an optimised ratio of 1:5, the NFs were found stable for a long duration compared to pure DIW-based NFs. Radkar et al. [12] examined the ZnO/DW NFs with a 9–15 nm NPs size and 0.05–0.25 vol % of NPs. It was found that the NFs were stable for the desired period. Different experimental findings elaborating the dispersion stability of ZnO/H_2O NFs and the techniques used to enhance the stability time are well reported in Table 1.

Numerous SFs for stability enhancement have been reported, but the literature still lacks information about optimising SFs concentrations. Most of the authors in the existing literature reported that the ZnO-based NFs, without any SFs, in an aqueous media possess poor dispersion stability. The standardisation of optimum ultrasonication time is another neglected area. The only possible solution to overcome stability-related issues is to treat NFs with both physical and chemical methods under optimised operating conditions.

1.2. Viscosity of nanofluids

The VC is another primary influencing parameter affecting the convective HTC and the flow properties of NFs in heat-exchanging mediums [17]. Its importance in the heat transfer thermal system is a critical point of consideration because it has a direct impact on the pumping power for the circulation of the NFs and directly influences the overall energy consumption of the system. Einstein [18] pioneered computing the viscosity of NFs with spherical-shaped NPs using classical hydrodynamic equations. The experimental findings reported in the literature confirmed that ZnO NFs' viscosity depends upon the NPs loading and operating temperature along with the other influencing parameters such as the morphology, pH, preparation techniques, nature and type of the stabilising agents.

Table 1
Dispersion stability of ZnO/H_2O-based NFs prepared using different techniques.

Nanofluids (NPs Size)	Stabilising Techniques	NPs/SFs Concentration	Operating Conditions	Stability (Days)	Ref
ZnO/DW + PVP (<100 nm)	Bath sonication (90 min)	NPs (0.30 vol %.),SFs (1.5 × NPs)	NFs stabilised with surfactant were found more stable compared to that pure NFs.	21	[13]
ZnO/DIW + SDBS + Brine (55 nm)	Magnetic stirring (60 min), Bath sonication (30–120 min)	NPs (0.1, wt. %.), SFs (0.017, 0.025, 0.050 wt %)	Sonication time = 60 min, pH = 2, SDBS concentration = 0.025 wt %,	12	[14]
ZnO/DW + XG (<50 nm)	Bath sonication (60 min)	NPs (0.1, 0.3, 0.5 wt %.), SFs (0.4 wt %)	SEM and DLS analysis showed the stability of NFs at 0.4 wt % of XG	3	[15]
ZnO/DW (−)	Magnetic stirring (15 min), Bath sonication (60 min)	NPs (0.05–0.1 wt %.)	0.1 wt % of NFs were stable, Maximum hydrodynamic size = 16 nm,	3	[16]

However, the existing literature lacks the effect of the aforementioned parameters [19]. Sadegh et al. [20] in their investigation observed that for graphene oxide-based NFs the behaviour of NFs changed from Newtonian to non-Newotonain with an increase in the mass concentrations of NPs. They also proposed a mathematical model, which predicted the findings of the study with reasonable accuracy under standard operating conditions. In another investigation [21], authors performed a study with magnetic NFs considering the wedge flow in the Eulerian framework to investigate the NFs' effectiveness. The study considered the NPs size, Brownian motion and thermophoresis effect within the NFs which were overlooked by popular classical models. The authors in their previous study [22] evaluated the viscosity of ZnO NFs under varying mass concentrations and operating temperatures. The findings showed an increasing trend with the NPs loading while an opposite behaviour was observed with the rise in the operating temperature. The findings were in line with the results of similar kinds of studies recorded in the existing literature. The experimental studies addressing the VC of ZnO/DIW NFs have been reported in Table 2 with and without using SFs under different NPs loadings and operating temperatures.

The reported literature has inconsistencies because of the non-standardisation of different methods used to prepare and measure the VC of NFs. Furthermore, the optimization of NPs size, concentration, and stabilising agents used is still a neglected area for an optimised viscosity of ZnO NFs in an aqueous media for potential heat transfer applications. However, it can be concluded that an optimised concentration and size of NPs, stable operating conditions, and SFs concentrations are possible ways to optimise the viscosity of NFs. It will not only lead towards the smooth operation of the heat exchanging systems but also result in a little compromise over the pressure drop and frictional losses and the system's overall energy consumption.

1.3. Thermal conductivity of nanofluids

NFs' TC is a critical controlling characteristic among the thermophysical properties, which depends upon the physiochemical characteristics of the NPs. ZnO NPs have anomalous high thermal conductivity similar to metal oxide NPs and have suitable heat transfer applications. Jeong et al. [27] analyzed the ammonium polymethacrylate stabilised ZnO/DIW NFs with NPs size 20–40 nm and reported an enhancement of up to 16% at 5.0 vol % in thermal conductivity for spherical shape NPs. This increase was 19.8% for rectangular-shaped NPs under the same operating conditions and NPs size 90–210 nm. The possible rise in the rectangular-shaped NPs may be due to larger particle sizes. Sadegh et al. [28] proposed empirical models for the estimation of TC of NFs based on the analytical data for the estimation of TC with reasonable accuracy in the absence of experimental tools. Different experimental thermal conductivity-related investigations of aqueous ZnO NFs under different NPs loadings and operating temperatures have been presented in Table 3.

It can be seen that ZnO NFs possess relatively good thermal properties and could be a potential HTF. The NPs with spherical shapes and smaller sizes have better thermal characteristics than large and non-spherical ones. However, there are several inconsistencies in the existing data regarding the impact of NPs concentration, nature, and type of SFs used. An optimised concentration and size of NPs, stable operating conditions, and SFs concentrations are possible ways to enhance the thermal properties of aqueous ZnO NFs for potential applications in different heat-exchanging systems.

1.4. Convective heat transfer of nanofluids

Zinc Oxide NFs possess remarkably high thermal and rheological characteristics for their potential heat transfer applications in conventional and compact channels. This is probably of the different sizes and shapes of NPs, the techniques used for the preparation and stability enhancement of NFs, and the conditions under which the fluid is tested. Numerous studies reporting the experimental findings from different research groups on the convective HTC of aqueous ZnO NFs in small-diameter circular cross-section tubes presented different results. Shahrul et al. [13], in their study with 0.3 vol % of PVP stabilised aqueous ZnO NFs, observed an improvement of 35% in the overall HTC. Sharifpur et al. [30] observed similar findings for aqueous ZnO NFs in a square cavity with a rise of 9.14% in convective HTC for 0.10 vol% of NPs. Topuz et al. [25] investigated SDS-stabilised ZnO NFs in an aqueous media flowing through a horizontal circular microchannel (Microtube, ID = 4 mm, 7.5 mm, 10 mm, length = 200 mm) under the constant surface temperature condition in laminar flow regime (Re = 500–2300). ZnO (18 nm) NPs with 0.5, 0.7 and 1.0 vol % concentration of NPs showed an improvement in HTC up to 1.5% only. In another experimental and numerical study [31], hydraulic characteristics of Al_2O_3 NFs were explored in a pours media. The small size of the NPs proved to be excellent not causing any kind of blockage within the flow system. Niknejadi et al. [32] in their experimental study with Fe_3O_4-based NFs analyzed the flow and thermal characteristics of NFs within a twisted tube. The findings showed that the performance of NFs was quite superior in the twisted tube when compared

Table 2
Viscosity of ZnO/H_2O-based NFs under various operating conditions.

Nanofluid (NPs Size)	NPs/SFs Concentration	Temperature (°C)	Test Method (Instrument)	Viscosity Enhancement	Ref
ZnO/DIW + SDS (100 nm)	NPs (0.01–1.0 wt %)	50–70	Ostwald type viscometer	Viscosity increased with the temperature and concentration of NPs.	[23]
ZnO/DIW (20–40 nm)	NPs (1.0–2.0 vol %)	30–90	Viscometer (LVDV II + Pro, Brookfield, USA).	Maximum enhancement of 68% for 2.0 vol % NPs at 90°C	[24]
ZnO/DW + SDS (18 nm)	NPs (0.5, 0.7, 1.0 vol %)	20–50	Viscometer (LVDV II + Pro, Brookfield, USA).	Maximum enhancement of 20% for 1.0 vol % NPs at 20°C	[25]
ZnO/DW (25 nm)	NPs(1.0, 1.5,2.0 vol %)	20–25	DV-II + PRO Digital Viscometer)	Maximum enhancement of 23% for 2.0 vol % of NPs at 25°C	[26]

Table 3
Thermal Conductivity of ZnO/H_2O-based NFs under various operating conditions.

Nanofluid (NPs Size)	NPs/SFs Concentration	Temperature (°C)	Test Method (Instrument)	Thermal conductivity Enhancement	Ref
ZnO/DIW (20–40 nm)	NPs (1.0–2.0 vol %)	30–90	KD2 Pro Thermal Analyzer (THW)	Enhancement of 8.0–15.0% for 1–2.0 vol % of NPs	[24]
ZnO/DW + SDS (18 nm)	NPs (0.5, 0.7, 1.0 vol %)	30–60	KD2 Pro Thermal Analyzer (THW)	Maximum enhancement of 9.0% at 30-60°C	[25]
ZnO/DW (25 nm)	NPs(1.0, 1.5,2.0 vol %)	25	KD2 Pro Thermal Analyzer (THW)	Enhancement of 12% for 2.0 vol % of NPs	[26]
ZnO/H_2O (30 & 60 nm)	NPs (1.0 vol %)	25	KD2 Pro Thermal Analyzer (THW)	Enhancement of 11.5 & 7.3 %for 30 nm and 60 nm NPs	[29]

with the results obtained from the plain tube. In another study [33] the flow behaviour of Fe_3O_4-based NFs was investigated in microchannels and it was found that the density, velocity and temperature of the NFs are also affected by the nature of the material of the microchannel. Karimi et al. [34] in their investigation of SiC/H_2O-based NFs observed that the thermal and hydraulic characteristics of NFs are directly influenced by the NPs loading and volume flow rate. An enhancement of 19.8% in HTC was found while operating with the NFs over the host BFs. Azimy et al. [35] conducted a study to investigate the impact of sonication waves on the thermal performance and stability of aqueous-based MWCNT NFs in the mini heat exchanger at varying Re number values were assessed experimentally. Their observation showed that the NFs' stability and HTC were dramatically increased by applying ultrasonic waves, but when the Re number increased, the effects of the sonication waves on NFs' stability and HTC decreased. Maximum HTC growth of 196% was recorded at 0.25 wt % of NPs and Re = 387 in comparison to water. The authors in one of their previous studies [36] also analyzed the impact of minichannel cross-sectional area on the HTC and pressure drop of aqueous ZnO NFs. The investigation revealed that smaller diameters resulting the smaller inlet cross sectional area of the minichannels are preferable for higher HTC, with a little compromise over the pressure drop across the test section.

Table 4 shows a few literature studies targeting the ZnO NFs heat transfer performance in an aqueous media in mini and microchannels under different operating conditions. The research results presented in Table 4 show that aqueous ZnO NFs have excellent potential for heat transfer augmentation in compact channels. It has been examined that considerable improvement in Nusselt number and frictional pressure drops can be attained with the rise in NPs loading and Reynolds number. But the increased NPs loading may result in particle aggregation, and more frictional pressure drops across the flow channel. Optimising the concentrations NPs and SFs, and flow rates for reduced pressure drops and frictional losses would further enhance ZnO NFs' potential in conventional and compact channels. The experimental and numerical findings in the existing literature have also shown that the combination of MCHEs and NFs has reasonably enhanced the heat transfer characteristics of BFs.

As per the literature, among the metal oxides, extensive studies exist with aqueous-based Al_2O_3, CuO, SiO_2, and TiO_2 NFs. In addition, limited experimental investigations have been reported on the thermal (thermal conductivity, local HTC, average HTC) and hydraulic (viscosity, pressure gradient, friction factor) performance of water-based zinc oxide (ZnO) NFs in minichannels. Among the reported studies, many researchers used different stabilising agents to attain enhanced dispersion stability of ZnO-based NFs in a variety of BFs [40]. However, none of these studies has reported the impact of stabilising agents on the thermal (thermal conductivity, local HTC, average HTC) and hydraulic (viscosity, pressure gradient, friction factor) performance of zinc oxide (ZnO)-based aqueous NFs at extremely-low NPs loading. Therefore, the current investigation examines the thermophysical properties, thermal performance, and hydraulic characteristics of aqueous zinc oxide (ZnO) based NFs in different NPs loading ranging from 0.012 to 0.048 wt with and without using SFs. In addition, the effect of thermophysical properties, SFs, the NPs concentration, and the fluid flow characteristics on the local and average HTC, along with the pressure gradient across the test section, and friction factor losses, have been investigated.

2. Materials and synthesis of nanofluids

Preparing NFs under desired operating conditions is challenging and generally synthesised using either a one-step or two-step technique. The present investigation has followed a standard two-step method for synthesising the aqueous ZnO NFs under steady-state standard working conditions [41].

Table 4
Heat transfer performance of ZnO/H_2O-based NFs under various operating conditions.

NFs/(NPs Size)/(Loading)	Geometry	Type of flow	Enhancement	Ref
ZnO/DIW, (20–100 nm)/ (0.82–0.93 vol%)	Straight tube, OD = 5.0 mm, ID = 4.0 mm, Length = 500 mm,	Type of flow: Laminar, Re = 200-15000	Heat transfer coefficient improvement to 8% and 3% for polygonal and rod-like NPs.	[37]
ZnO/DW, (25 nm)/(1.0, 1.5, 2.0 vol%)	Straight tube, OD = 2.5 mm, ID = 1.5 mm, Length = 500 mm,	Type of flow: Laminar, Re = 200-1800	The rise in heat transfer was recorded as 3.623 at 2.0 vol% of NPs at Re = 1800	[26]
ZnO/DIW, (30, 40, 50 nm)/ (1.0, 1.5, 2.0 vol%)	Rectangular Microhannel, Height = 400 μm, Width = 200 μm, Length = 10 mm	Type of flow: Laminar, Re = 1300	The average Nusselt number increased 0.44% at 2.0 vol% and NPs of 30 nm.	[38]
ZnO/DIW, (20–40 nm)/ (0–10 vol%)	Straight tube, OD = 1.0 mm, ID = 0.5 mm, Length = 300 mm	Type of flow: Laminar, Re = 25-1500	Almost 3.2% rise in Nusselt number was found at the same concentration of NPs and Re	[39]

2.1. Nanoparticles and stabilising agents

In the current investigation, dry ZnO NPs, ACAC and SHMP were procured from Nanostructured and Amorphous Materials, Merck, Riedel Haën. Highly purified DIW was purchased locally. Numerous characteristic properties of the subject NPs and SFs are enlisted in Table 5.

2.2. Synthesis methods of ZnO NFs

Aqueous ZnO NFs were prepared in 0.012–0.048% mass concentrations with and without stabilising agents, using magnetic stirring (Heidolph MR Hei-End) followed by bath ultrasonication (Elma E100H) under optimised operating conditions.

The experimental scheme for preparing NFs is well elaborated in Fig. 1. A precise analytical micro-balance (AWU-220D Shimadzu) was used for the mass measurement of NPs. The system's temperature was controlled using TC-550MX, a thermal bath with enhanced precision, to maintain the system's accurate temperature. The detailed specifications of the instruments are elaborated on in our previous study [42]. SHMP and ACAC were used as stabilising agents. The NFs preparation was carried out using an optimised stirring of 1 h and sonication of 3 h, optimization procedure has been reported in an earlier study [42] from the group when experimental campaign was carried out at our previous study, at a constant temperature of 30 °C.The stirrer rpm was adjusted at 1000, while the sonication frequency and power was 37 kHz and 150 W, respectively. For the preparation of SFs stabilised NFs, after aforementioned procedure the stabilising agents were added to the prepared NFs. The optimum concentrations of SHMP and ACAC were identified by testing various concentrations of stabilising agents and NP's, the details can be tracked/traced from an earlier reported work from the group [42]. The findings from earlier work showed that under optimised operating conditions and SFs concentrations, the nanofluid samples reamined stable for 24, 48, and 96 h for pure, SHMP, and ACAC-based NFs, respectively. The optimised concentrations of stabilising agents and the NPs are well detailed in Table 6. To ease results interpretation, different abbreviations for pure and SFs stabilised aqueous ZnO NFs have been used in Table 6. The NPs and SHMP are in mg, while ACAC is in μl.

For this study, addition of stabilising agents has enhanced the dispersion stability of NFs. The dissociation of the SHMP into Na^{+} and PO^{3-} ions and the chemisorption of the phosphate ions on the NP's surface discourage the aggregation of NPs within the host BFs. It was also observed that the SHMP possessed a linear relationship with the concentration of the ZnO NPs. On the other hand, while dealing with ACAC-stabilised NFs, formulation of weak chelating complex breaks the NPs aggregates to their original size leading towards uniform dispersion of NPs within the host BFs. The concentration of ACAC and ZnO NPs possessed a direct proportion, however, a nonlinear trend has been observed between both in the present study.

3. Characterisation of nanoparticles

In the current research investigation, the morphological characteristics, chemical composition, crystal structure, and specific surface area (SSA) of dry ZnO NPs were measured using the instruments, presented with their detailed specifications, accuracy, and limitations in our previous study [42].

3.1. SEM and EDX study of NPs

The morphological characteristics of ZnO NPs revealed that the NPs were randomly distributed, nearly spherical, and particle diameter was around 16–40 nm. The images collected from various sample holder locations showed a slight aggregation of NPs, as shown in Fig. 2 (a) and 2 (b). The Energy Dispersive X- Rays Spectroscopy (EDX) analysis, as presented in Fig. 3 (a), showed the average mass concentration was 80.45% and 19.45% for "Zn" and "O", respectively.

3.2. XRD and BET analysis of NPs

The XRD characterisation of dry ZnO NPs, presented in Fig. 3 (b), showed a monoclinic structure and is well mapped with the JCPDS card No. 36–1451. It implies the excellent crystalline nature of ZnO NPs. The enlargement peaks on the lowermost side reflect the small and nanometric crystal sizes of the NPs [43]. The nanometric crystal size of the NPs shows their excellent suitability for the preparation of NFs, and their potential use for heat removal from high heat flux thermal systems.

The BET SSA area ZnO NPs were found as 22.37 m^2/g, while the true density of the NPs, as recorded with a gas pycnometer, was 6.850 g/m^3, which slightly differed from the theoretical value (5.606 g/m^3) as reported in the literature, possibly due to the aggregation effect during the storage of NPs [44]. Therefore, the aggregation of the NPs during storage and transportation could be the possible cause for the change in SSA than the manufacturer specification.

Table 5
Properties of ZnO NPs and SFs at standard temperature and pressure (STP).

Material	Appearance	Size	Specific Heat	Thermal Conductivity	pH	Density	SSA	Purity
ZnO	White	20 nm	514 (J/kgK)	29.00 (W/m.K)	6.5–7.5	6850 kg/m^3	40 m^2/g	99.5%
SHMP	White	–	–	–	8.6	2480 kg/m^3	–	97.0%
ACAC	Coluorless	–	–	–	6.0	975 kg/m^3	–	99.0%

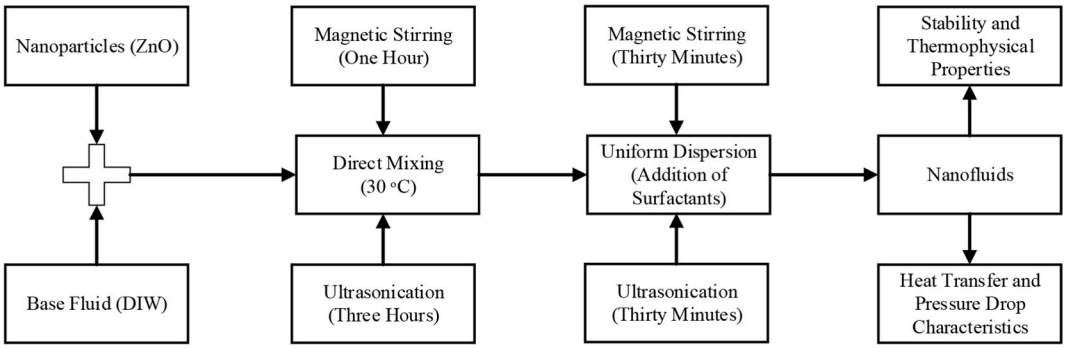

Fig. 1. Experimental scheme and procedure for the preparation of Pure and SFs stabilised ZnO NFs in an aqueous media for the analysis of their thermal and hydraulic properties.

Table 6
Abbreviations and NPs and SFs concentrations used to prepare aqueous ZnO NFs.

NPs (wt. %)	ZnO + DIW	ZnO + DIW + SHMP		ZnO + DIW + ACAC	
0.012	Z12P	Z12S	NPs:SHMP 2:1	Z12A	NPs:ACAC 16.66:1
0.024	Z24P	Z24S	NPs: SHMP 2:1	Z24A	NPs: ACAC 12.50:1
0.036	Z36P	Z36S	NPs: SHMP 2:1	Z36A	NPs: ACAC 10.00:1
0.048	Z48P	Z48S	NPs: SHMP 2:1	Z48A	NPs: ACAC 8.34:1

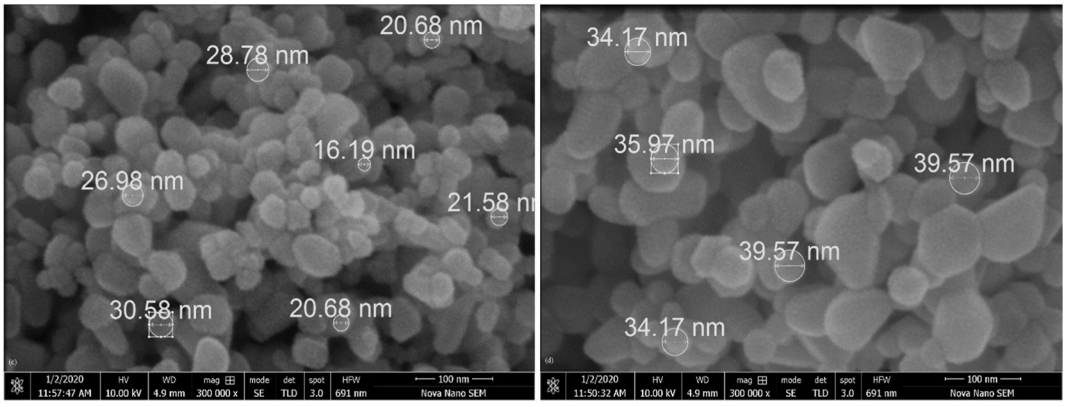

Fig. 2. SEM characterization of ZnO NPs (a) 16–30 nm (d) 30–40 nm.

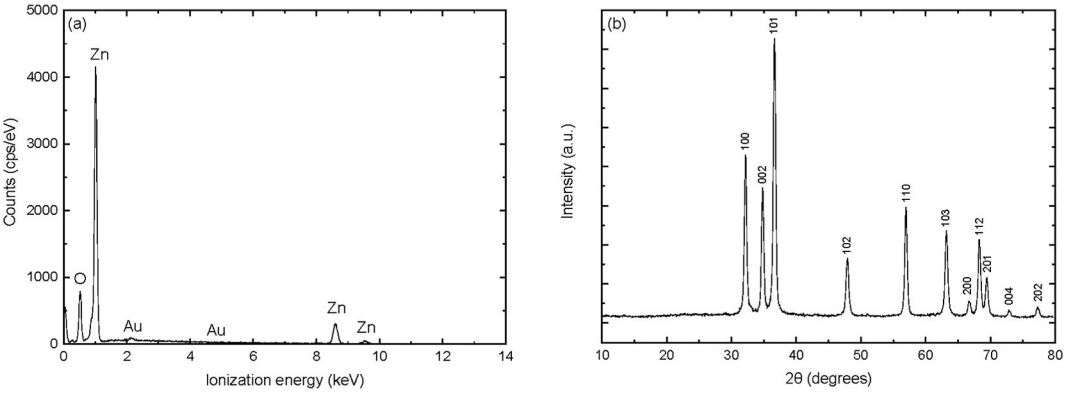

Fig. 3. Characterisation of dry ZnO NPs (a) EDX Analysis (b) XRD Analysis.

4. Experimental test setup and methods

4.1. Viscosity estimation of NFs

The hydraulic performance of the NFs within the compact channel heat exchanging systems is greatly influenced by the rheological characteristic of the NFs, NPs loading and operating temperatures are observed to be the key controlling parameters. The viscosity of NFs measured by estimating the ratio between the applied shear rate and the corresponding shear stress within the NFs system [45]. The viscosity of the NFs was estimated using a Rotary Rheometer (RHEOTEST® RN 5.1). A measured quantity of about 35 ml was filled in measuring cup G1 having a diameter of 38 mm. A rotor S1 possing a diameter of 35.04 mm and height of 52.56 mm was inserted in the cup and the whole assembly was locked for the execution of the test. The system was connected to a thermal bath for maintaining the desired temperature. In the current study, the operating temperature was varied within 20–60 °C. The whole system was connected with a data acquisition system to set and adjust the desired operating conditions. The detailed specifications of the rheometer used are presented in our previous study [42]. The system's maximum viscosity measuring range was between 1 and 3×10^9 mPas, with an adjustable shear rate of 0–1300 s^{-1}. Using the operating system RHEOTEST® RN 5.1, the shear rate was adjusted from 0 to 1000 s^{-1}. The system was then run under the desired set of operating conditions for the execution of the data. The procedure was repeated for the VC measurement by changing the set temperature and NPs loading within the subject shear rate range to analyze the effect of temperature and NPs concentration. The system's accuracy was up to ±1.0%, and the system was calibrated every week using a standard solution of known viscosity.

4.2. Thermal conductivity estimation of NFs

The present experimental investigation examined the TC of ZnO/DIW-based NFs using a unique TC analyser (TEMPOS, Meter Group, USA). A stainless steel sensor (KS-3) is used to simultaneously apply a small amount of heat in the NFs to investigate the TC by estimating the heat conduction capability of the NFs. The sensor simultaneously acts as a heat source and sensor and has a measuring TC range of 0.02–2 W/m.K. The calibration of the sensor using a standard glycerine solution showed experimental accuracy of the instrument within ±1.0%. A set of 4–6 experimental readings was recorded for accurate measurement of thermal conductivity, and then finally, an average of all the readings was used for final analysis. All the measurements were recorded under controlled temperature conditions within 20–60 °C.

4.3. Experimental heat transfer section

The present experimental work was conducted in a laminar flow to examine the convective HTC and pressure drop properties of aqueous-based ZnO NFs under standard steady-state operating conditions in a minichannel comprising a very small diameter test tube. The setup was subjected to electrical heating using a variable current and voltage DC power supply. The DC power supply (LONG WEI, LW3060KD) has precise control of the current and the voltage to maintain constant heat flux boundary conditions at the outer surface of the test section wall. The collected data was later analyzed to clarify the effect of applied heat flux, the NPs concentrations, and the fluid flow rates on the HTC of NFs in a compact channel. The experimental setup used in the present investigation is presented in Fig. 4. All the components of the setup have been labelled as shown in Fig. 4. The graphical diagram of the convective heat transfer minichannel test setup and its instrumentation is shown in Fig. 5. The experimental test setup is a stainless-steel mini-tube (ID = 1.0 mm, OD = 1.5 mm, L = 330 mm), with an effective heated length of 280 mm. The whole system was adequately insulated to avoid environmental effects and heat losses to the ambient. A Legato 200 KDS infuse-only dual syringe pump with excellent accuracy for precise control of fluid flow rate was used in this study. The experiments were carried out by varying the volume flow rate of the NFs within the minichannel test setup from 12.0 to 24.0 ml/min for all tested conditions. To measure the outer wall surface temperature of the minichannel test section, 10 K-type temperature sensors were used. These sensors were attached with Omega OB-101-1 epoxy, which makes it possible a good thermal contact and weak electrical contact of the thermocouples with the test section outer wall surface for the accurate measurement of the temperatures. Two additional thermocouples were placed at the entry section and the outlet region of the minichannel test tube to estimate and measure the temperatures of the entering accurately and exiting fluids. All thermocouples in a reference bath were calibrated in a 20–60 °C temperature range. The maximum uncertainty recorded in the temperature was ±0.1°C.

The volume flow rate of the NFs passing through the minichannel test section was cross-verified using a digital analytical mass balance with ±0.01 g accuracy. The difference in the measured values and those cross-verified from the mass balance was less than

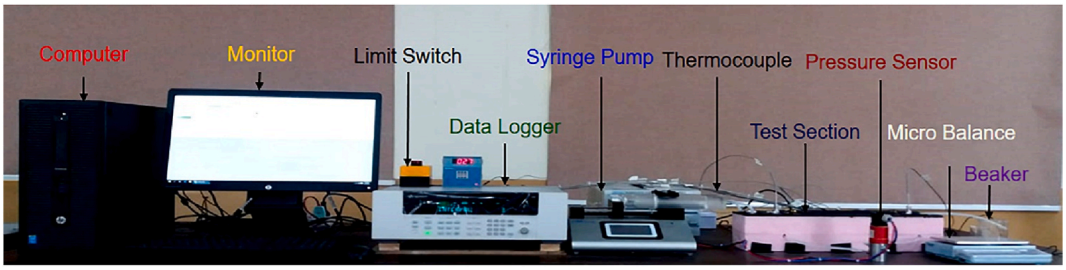

Fig. 4. Experimental setup for the investigation of the thermohydraulic performance of ZnO NFs.

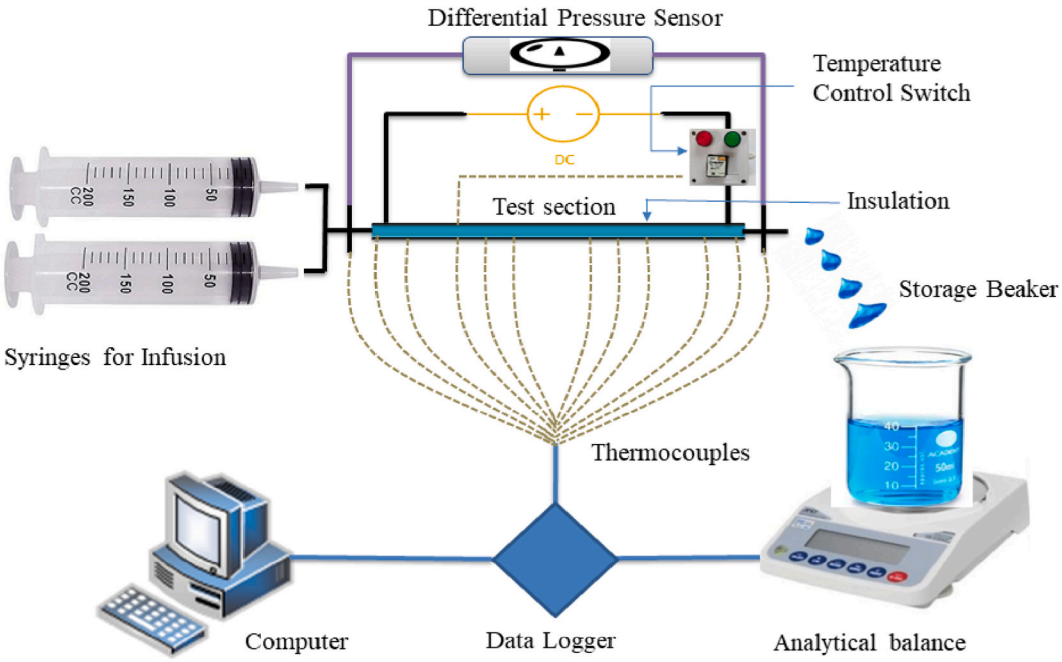

Fig. 5. Schematic of minichannel test rig for the investigation of the thermohydraulic performance of ZnO/DIW NFs.

1.0%. The pressure gradient across the test tube inlet and outlet is essential for estimating the system's required power input and corresponding energy consumption. This investigation measured the pressure gradient across the minichannel test section using a highly precise differential pressure gauge (HC 692, Range 0–1 bar).

The pressure transducer possesses an accuracy of ±1.25%. To record the experimental data set from the temperature sensors and the pressure transducer, a data acquisition system (Keysight 34970A) was used. The experimental data were recorded after an interval of 5s each when the system attained a steady state condition. Detailed specifications of used instruments with their accuracies and other limitations are provided in Table 7 and are also available in a study [36] conducted by the authors.

4.4. Heat transfer calculations

The thermal and hydraulic performance of the NFs can be investigated either under constant heat flux or constant wall temperature boundary conditions depending upon the nature of the heat exchanging system [46]. In the present experimental study, the heat transfer and pressure drop properties of the NFs were investigated under constant heat flux boundary conditions for the aforementioned NPs loadings and fluid flow conditions.

Thermal conductivity, viscosity, and density of NFs should be well-known before conducting experiments related to convective HTC. Before proceeding with the exact estimation of the NF's pressure gradient across the test section and the frictional losses during the fluid flow within the minichannel heat exchanging system, these parameters must be known. Therefore, the volume concentration of NPs in the NFs was calculated using equation (1).

$$\varphi \times 100 = \frac{m_{np}}{\rho_{np}} \Big/ \frac{m_{np}}{\rho_{np}} + \frac{m_{bf}}{\rho_{bf}} \tag{1}$$

The density measurement of NFs was crucial, and a highly sensitive system was needed for its experimental investigation. The density of NFs was estimated by mixing theory [47] using equation (2), primarily depending upon the density of BFs, NPs, and the

Table 7
Specifications of adjustable DC power supply and syringe pump.

Name	Model	Specifications
Adjustable DC power supply	LONG WEI LW3060KD	Output Voltage Range: 0–60V, Voltage Stabilization: ≤0.2%, Output Current Range: 0–30A, Current Stabilization: ≤0.5%, Display Accuracy: ±1% ± 1 digit
Syringe pump	Legato KDS 200	Flow Rate (Minimum): 5 pl/min, Flow Rate (Maximum): 215.803 ml/min, Power: 100–240 VAC: 50/60 Hz, 50 W, Accuracy:±0.35%
Thermally conductive epoxy	Omega OB-101-1/2	Maximum continuous temperature: 105 °C, Work-life: 30 min at room temperature, Thermal conductivity: high, Electrical insulation: Very high
Differential pressure transducer	Huba Control 692	Differential pressure range: 0–1 bar, Medium: Liquids and natural gases, Operating temperature: 15-85 °C, accuracy, and repeatability: ±1.25%

concentration of NPs.

$$\rho_{nf} = \varphi\rho_{np} + (1-\varphi)\rho_{bf} \tag{2}$$

The specific heat "c_p" [48] was estimated with equation (3), where the subscript of "np" and "nf" means NPs and NFs, φ is a volume fraction.

$$\rho_{nf}\left(c_p\right)_{nf} = \varphi\left(\rho c_p\right)_{np} + (1-\varphi)\ \left(\rho c_p\right)_{bf} \tag{3}$$

The local convective HTC "h(x)" was estimated from the total surface area of the minichannel test section, the applied power, the outer wall surface temperature and the bulk fluid temperature, as clarified in equation (4):

$$h(x) = \frac{Q}{A.\left(T_{s-in.x} - T_{f.x}\right)} = \frac{\ddot{q}}{\left(T_{s-in.x} - T_{f.x}\right)} \tag{4}$$

The heat input of "Q" was calculated by the electricity fed into the test section, and a multimeter was used to estimate injected electricity. Where "$\ddot{q}$" is the applied heat flux, "x" is the distance in the axial direction across the mini tube, and T_s and T_f are the tube wall and mean bulk fluid temperatures, respectively. The inner wall temperature of the minichannel test section can be estimated using equation (5), where φ is the $(D_{out}/D_{in})^2$.

$$T_{s-in,s} = T_{s-out,x} + \frac{Q}{4\pi L k_{tube}}\left[\frac{\varphi(1-\varphi)-1}{\varphi-1}\right] \tag{5}$$

The fluid temperature at any local position along the flow was estimated with an energy balance approach, equation (6) was used for this estimation;

$$T_{f,x} = T_{in} + \frac{\ddot{q}\pi D_i x}{\dot{m}c_p} \tag{6}$$

The theoretical average Nusselt number can be estimated with Shah's correlation [49]; the formulation is given in equation (7). For the present experimental investigation under the applied test conditions, the average Nusselt number was estimated by averaging the local Nusselt number across the length of the test section.

$$Nu_{avg} = \begin{cases} 1.953L*^{-1/3}\ L* \le 0.03 \\ 4.364 + 0.0722L^{*-1}\ L* > 0.03 \end{cases} \tag{7}$$

Where "L*" is the non-dimensional length and can be calculated using a correlation $(L/D_{in})/(RePr)$. The average HTC can then be estimated using the correlation in equation (8), where "k" is the TC of the NFs.

$$Nu(x) = \frac{h(x)D_i}{k} \tag{8}$$

The friction factor can be assessed using correlation [50] as given in equation (9) when the flow is fully laminar and in the developed region.

$$f = \frac{64}{Re} \tag{9}$$

The friction factor within the laminar regime is based on the Darcy Weisbach correlation [50], and its formulation is given in equation (10).

$$f = \frac{2\Delta\ PD_i}{L\rho u_m^2} \tag{10}$$

Here "ρ" is the density of the fluid, "u_m" is the mean velocity of the fluid, "L" and "D_i" are the characteristic length and the inner wall diameter of the system under consideration, respectively. The differential pressure was measured experimentally and theoretically [50] using equation (11) less than the theoretical values.

$$\Delta\ P = \frac{32LRe\mu^2}{\rho D_i^3} = \frac{32Lu_m\mu}{D_i^2} \tag{11}$$

The theoretical pumping power (P) across the flow channel for maintaining the desired flow rate of the fluid is presented in equation (12).

$$P = V\Delta\ P \tag{12}$$

In this correlation, the fluid volume flow rate is presented by "V," while ΔP is the pressure gradient across the channel under consideration.

4.5. Uncertainty of measured parameters

The associated uncertainty levels of the independent and dependent variables in any experimental study define the reliability and

reproducibility of experimental results. Therefore, type B uncertainty in experimental results reported in this study was estimated following Moffat's procedure [51]. The core purpose is finding the uncertainty in the computed values using the information from original measured parameters. The uncertainty in the calculated values can be easily measured using the root sum square method, and the results are expected to be as accurate as the original input parameters. For a single measured value, the uncertainty could be represented as $\delta z_{xi} = (\delta f/\delta xi)\delta xi$. For several independent input parameters, the individual variables are summarized by the root sum square method as presented in equation (13).

$$\Delta z = \pm \sqrt{\sum_{i-1}^{n} \left(\frac{\vartheta f}{\vartheta x_i}\right)^2 (\Delta x_i)^2} \tag{13}$$

This is the basic equation of uncertainty analysis possessing multiple variables. Each term represents the contribution made by the uncertainty in one variable, δx_i, to the overall uncertainty in the result, Δz. Each term has the same form, the partial derivative of $f(x)$ concerning x_i multiplied by the uncertainty interval for that variable. The uncertainties of important dependent and independent parameters are enlisted in Table 8. The low uncertainties in the dependent and independent variables confirm the excellent accuracy of the experimental setups.

The projected uncertainties would possessed the same probability as possessed by the independent individual results. equation (13), would be applicable to the independent variables, and would display the Gaussian distributions for the repaeated results at the same odds.

5. Results and discussion

This section consists of the research findings investigated for thermal conductivity, viscosity, HTC, and pressure drop across the test section for ZnO NFs in a given concentration of NPs, operating temperatures, and flow rates under steady-state stable set conditions.

5.1. Viscosity estimation of ZnO NFs

The experimental absolute VC and VC ratio of pure and SFs stabilised ZnO NFs in an aqueous media has been presented in Fig. 6 (a) and 6 (b). As shown in Fig. 6 (a), the VC of the NFs, showed a significant dependency on the operating temperature and NPs loading. It followed a direct proportion with the NPs concentration, while an inverse behaviour is observed with the temperature rise.

The viscosity increase at a fixed temperature (30 °C) was 12.82%, 16.38%, and 14.39% for pure DIW, SHMP, and ACAC-based NFs, respectively, as indicated in Fig. 6 (b). The highest viscosity possessed by SHMP stabilised NFs attributes towards the comparatively higher specific gravity and bulk density of SHMP than that of DIW compared to ACAC. It can also be seen that there is little difference between the VC of the pure DIW-based and ACAC-stabilised NFs. However, the prolonged dispersion stability of the ACAC-based NFs over the pure DIW-based NFs makes them more suitable for thermal applications, when the other thermophysical properties of the NFs are not compromised. The existing literature [52] supports the present study's behaviour observed with tested NFs. The VC decrement with the temperature rise contributes towards weakening the van der Waals forces between the adjoining NPs in the BFs, and the resistance between the adjacent layers of the fluid decreases. It also shows the suitability of the NFs for high heat flux thermal applications at elevated temperatures.

The current study's findings conclude that although the VC of NFs is affected by adding NPs and stabilising agents, the impact of stabilising agents was insignificant compared with DIW. The enhanced stability of SFs stabilised NFs proved that the NFs can be used effectively for high heat flux thermal systems while understanding their thermal properties with a bit of compromise over the cumulative VC effects on the hydraulic performance of the NFs.

5.2. Thermal conductivity estimation of ZnO NFs

The estimated TC and TC ratio of pure and SFs stabilised ZnO NFs in an aqueous media is presented in Fig. 7 (a) and 7 (b). Fig. 7 (a) shows the temperature and NPs loading-dependent TC of NFs, while Fig. 7 (b) presents the TC ratio change with the working temperature of the NFs. Both the TC and TC ratio of the NFs showed a strong direct dependency on NPs loading and the NF's temperature.

The TC increase at a fixed temperature (30 °C) was 18.63%, 23.70%, and 15.33% for pure DIW, SHMP, and ACAC-based ZnO NFs, respectively, as indicated in Fig. 7 (b). With the increase in NPs loading, the overall TC increased because of NPs higher TC in the host BFs. However, the rise in TC as a function of operating temperature enhances NPs' Brownian motion within the NFs dispersion [53].

Table 8
Measured uncertainties of different influential factors.

Independent Variables (Parameters)	Uncertainty (%)	Dependent Variables (Parameters)	Uncertainty (%)
Mass Flow Rate ($\dot{m}$)	1.0%	Surface Area (A_s)	1.04%
Length (L)	±1.0 mm	Friction factor (f)	5.25%
Diameter (D)	±0.01 mm	Pumping Power (P)	1.89%
Thermal conductivity (k)	±1.0%	Fluids velocity (u)	2.45%
Viscosity (μ)	±1.0%	Reynolds Number (Re)	1.73%
Density (ρ)	±1.0%	Local HTC (h_{local})	5.15%
Specific Heat Capacity (c_p)	±1.0%	Average HTC (h_{avg})	3.60%
Temperature (T)	±0.1 °C	Local *Nu* (Nu_{local})	5.34%
Pressure difference (ΔP)	1.25%	Average *Nu* (Nu_{avg})	4.20%

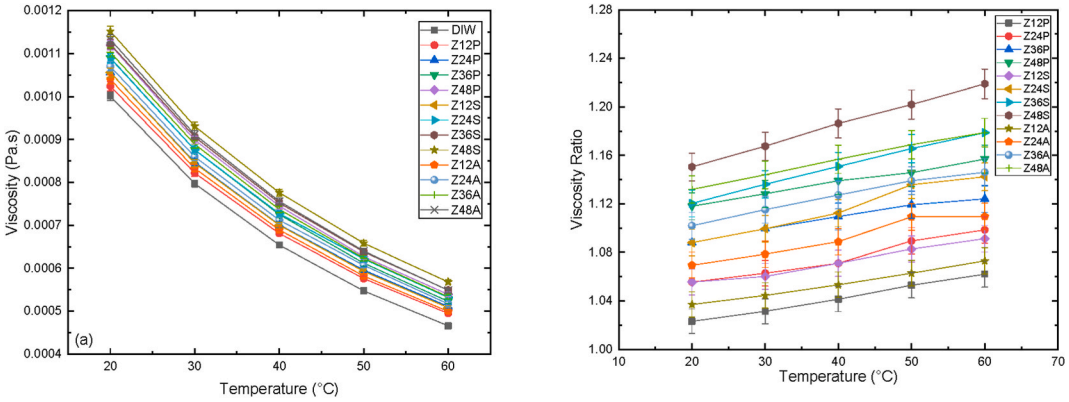

Fig. 6. ZnO NFs VC with the temperature change and NPs mass concentration (a) absolute VC (b) VC ratio.

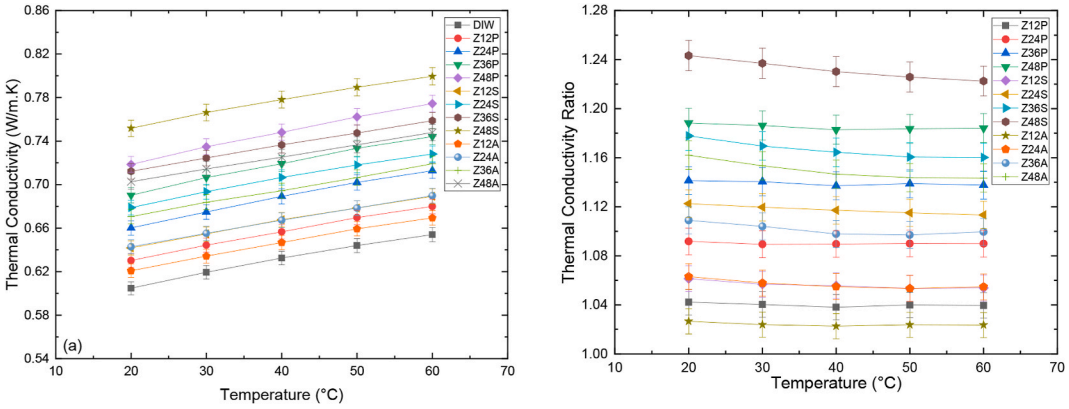

Fig. 7. Temperature-dependent ZnO NFs (a) absolute thermal conductivity (b) thermal conductivity ratio.

Therefore, the highest TC recorded for SHMP-stabilised NFs contributes to comparatively higher stability and the impact of SHMP's TC. The existing literature supports [54] NFs' dependency on the operating temperature and the NP's loading in the present study. The findings show that SHMP-based NFs could be an excellent potential candidate for thermal applications with a little compromise over the hydraulic performance in comparison to the pure DIW-based and ACAC-based NFs.

The experimental findings show that with the temperature variation, the TC change showed a similar trend at each concentration of NPs compared to DIW. This fact also strengthens the belief that temperature variations do not have any adverse or irregular effects on the thermal performance of NFs. Furthermore, it shows that the NFs' TC was systematically related to the operating temperature.

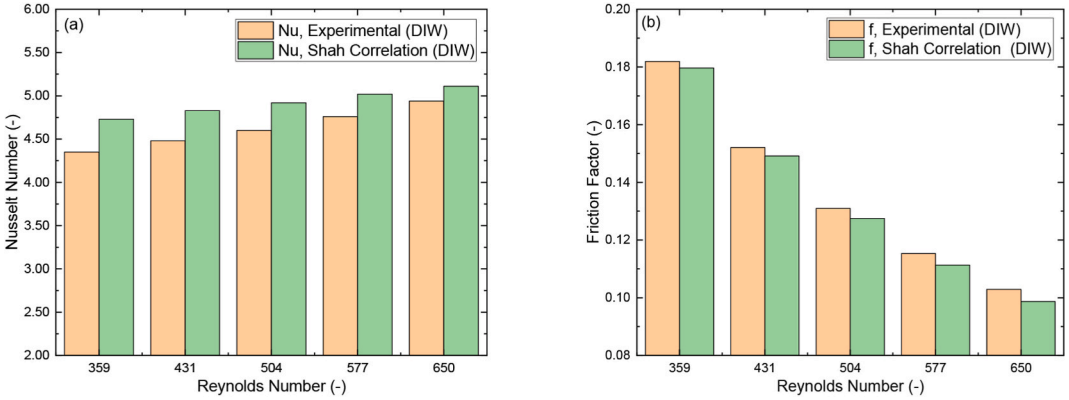

Fig. 8. Comparison of DIW at varying Reynolds numbers for (a) Nusselt number and (b) Friction factor.

5.3. Convective heat transfer coefficient of ZnO NFs

In the current investigation to evaluate the reliability of the test setup, first, a set of experiments were conducted with DIW within 12–24 ml/min. Then, the experimental findings with pure water were evaluated and compared with theoretical (Shah) correlations [49] for average Nusselt number and friction factor, as shown in Fig. 8 (a) and 8 (b), and the maximum deviations were within ±7.0% and ±4.0%, respectively.

The variation was significant at the first and last points because of axial conduction and the exact heating point along the tube test section. In addition, there is a high heat transfer rate because of irregularities and unsteady state conditions of the liquid at the entry region. Also, the fluid is developing in the entry section of the test setup and the velocity and the thermal boundary layers are not fully developed at this stage. Hence, the fluid is not in a fully steady state and the temperature fluctuations between the test set wall and the fluid are not stable.

The thermal properties of the NFs are supposed to be promising in the entire region due to the aforementioned effects. However, the system attains a steady state as long as the fluid flow leads towards the developing region. Consequently, the findings showed that the

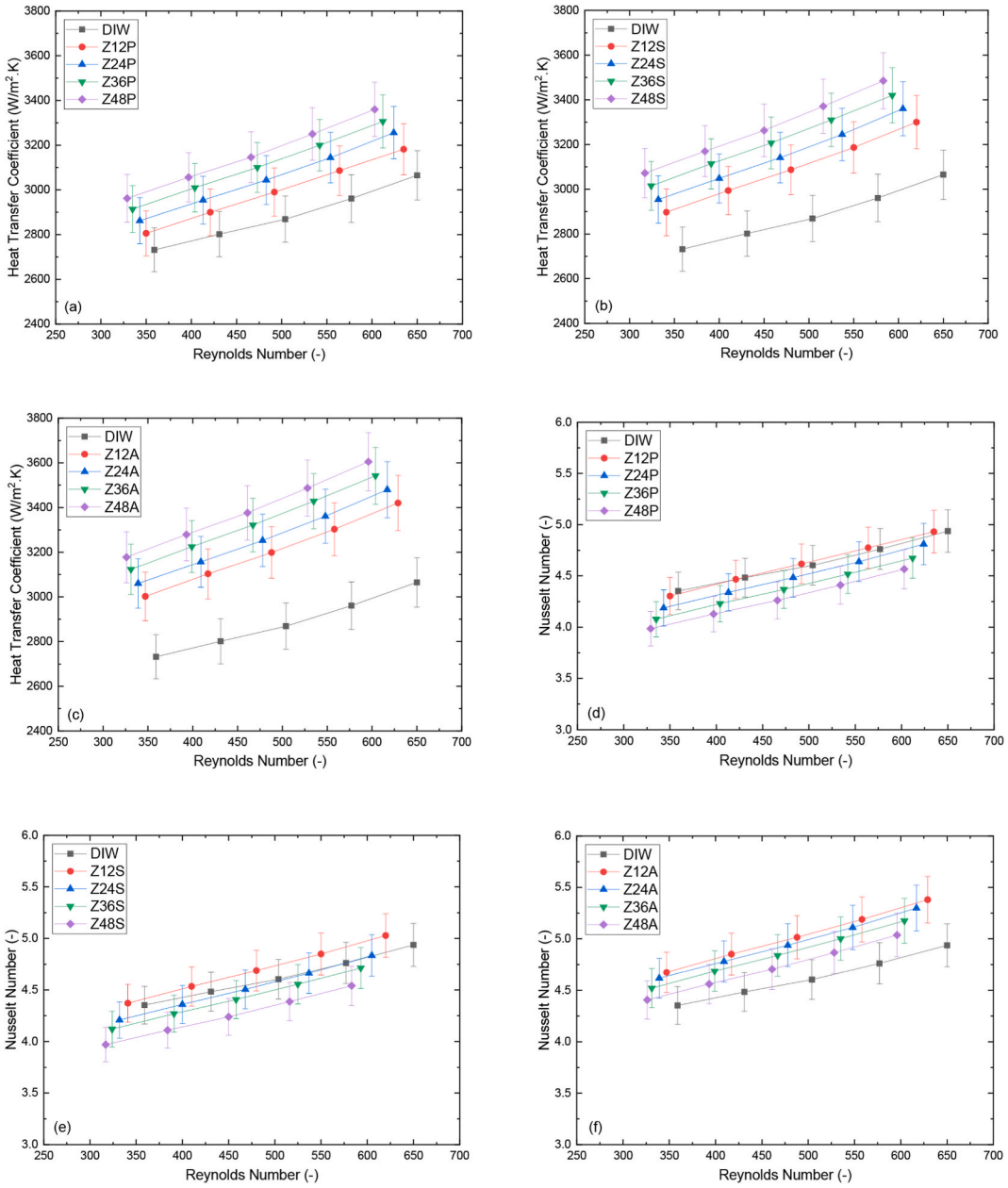

Fig. 9. Comparison of Convective HTC and Nusselt Number of ZnO NFs at different Reynolds Numbers (a) Pure NFs (b) SHMP basedNFs (c) ACAC-based NFs (d) Pure NFs (e) SHMP-based NFs (f) ACAC based NFs.

test setup was accurately performed and analyzed the comparative tests with the NFs.

It can also be seen that at higher Reynold Numbers the difference in the experimental and theoretical values for the Nusselt number is not much significant. However, slight changes have been observed for the friction factor with the variation in volume flow rates.

Fig. 9 depicts the change in the average heat transfer coefficient (HTC) and the Nusselt number (*Nu*) of aqueous ZnO NFs at varying mass concentrations of NPs and Reynolds numbers. Fig. 9 (a) to 9 (c) show the strong dependency of the average HTC over the NPs loading and Reynold number. The rise in the HTC for Pure DIW, SHMP and ACAC NFs was found to be 9.0%, 13.0% and 17.0% for Z48P ($Re = 603$), Z48S ($Re = 583$) and Z48A ($Re = 596$), respectively as shown in Fig. 9 (a) to 9 (c).

The Reynolds number was controlled with varying flow rates of NFs in 12–24 ml/min. The increase in HTC with the NP's loading is possibly due to the TC augmentation effects of adding NPs in the host BFs. For SHMP-stabilised NFs, the rise in average HTC was comparatively more than pure DIW-based ZnO NFs under the same operating conditions. The possible reasons for this enhancement are the uniform dispersion stability of SHMP-based NFs, and the TC rises due to adding NPs.

The research investigations with ACAC-based NFs presented better results than all the reported cases, and a maximum HTC enhancement has been observed. As already discussed in section 5.2, the addition of ACAC deteriorated the overall thermal conductivity of NFs to some extent. However, the enhanced HTC in the case of ACAC stabilised NFs also confirmed that the only aspect considered for improved HTC is not only the thermal conductivity of NFs but other parameters are also involved.

In the present case, the maximum enhancement in the HTC is also possibly due to enhanced Brownian motion of NPs, because the ACAC-based NFs were found most stable. Also, the VC of NFs was less effective than SHMP-based NFs, as explained in section 5.1. A similar trend has been seen in Fig. 9 (d) to Fig. 9 (f), where the average Nusselt Number is augmented with the volume flow rate while a depreciating effect was observed with NPs loading in almost all cases.

The maximum change in the average Nusselt number for Pure, SHMP, and ACAC-based NFs was found to be 7.50%, 8.10%, and 2.02% for Z48P ($Re = 603$), Z48S ($Re = 583$), and Z48A ($Re = 596$), respectively as shown in Fig. 9 (d) to Fig. 9 (f). The results revealed that the Brownian motion and TC augmentation are the most influencing parameters affecting the convective HTC of NFs. The addition of SFs positively influenced the system's overall performance by influencing the subject's two parameters.

5.4. Pressure gradient and friction factor of nanofluids

Fig. 10 presents the experimental findings depicting the pressure drop and the fictional losses across the minichannel test section under varying fluid flow rate conditions. In addition, the research analysis showed the NFs flow rate and NPs loading dependency of the pressure gradient and friction factor.

The maximum rise in pressure drop across the test section for Pure, SHMP, and ACAC-based NFs was 12.0%, 16.0%, and 13.0% for Z48P, Z48S, and Z48A, respectively, shown in Fig. 10(a–c). Friction factor losses across the test sections are directly linked with the pressure drop characteristics of NFs across the mini tube test channel. The pressure gradient increased with the concentrations of NPs and the Reynolds number. For all the tested NFs, the maximum pressure drop across the minichannel was recorded for SHMP-stabilised NFs corresponding to the pure DIW and ACAC-stabilised NFs. This fact attributes that the HTC augmentation is a little compromised with the addition of NPs because of pressure drop and consequently increased energy consumption by the pumping system.

As recorded and observed for the pressure gradient, a similar kind of trend was observed for the friction factor, as shown in Fig. 10 (d–f). The maximum rise in friction factor across the test section was 7.0%, 12.0%, and 9.0% for Z48P, Z48S, and Z48A, respectively, as shown in Fig. 10(d–f). The friction factor increased with the concentrations of NPs and the change in Reynolds number of NFs. The friction factor was maximum for SHMP-based NFs for all the tested cases.

Controlling the pressure gradient across the test setup could cope with the frictional losses across the test section for improved system heat transfer. Fig. 10 shows that the pressure gradient and frictional losses of aqueous ZnO NFs are higher than DIW across the test section. The maximum losses were observed for SHMP-based NFs. However, ACAC-based NFs possess minor changes relative to pure aqueous NFs. The pressure losses are directly proportional to the pumping power, which increases as the pressure drop increases, as more power is required to cope with the pressure losses.

Therefore, the author used the possible lower concentrations of NPs to prepare the aqueous NFs to cope with the issue to minimise the compromise over heat transfer characteristics of NFs, due to increased energy consumption used to cope with these losses.

6. Conclusions and future recommendations

The current investigation evaluated the thermophysical (viscosity, thermal conductivity) properties of ZnO NFs within 20–60 °C. The investigation was conducted using a minichannel test tube under constant wall heat flux in a laminar flow regime. The experimental findings led to the following conclusions.

1. Viscosity and thermal conductivity both showed an intense temperature and NPs loading dependency. The VC and TC were directly proportional to the operating temperature; however, in contrast to thermal conductivity, viscosity decreased with an increased operating temperature.
2. The maximum VC and TC rise for pure, SHMP, and ACAC-based ZnO NFs was recorded as 12.82–16.75% and 15.33–23.70%, respectively. The slight increase in VC and enhanced TC of NFs make them suitable for heat transfer in mini channels.
3. The HTC of NFs increased with the concentration of NPs. At a fixed volume flow rate of NFs, the enhancement in the HTC for Pure, SHMP, and ACAC-based NFs was 9.0%, 13.0%, and 17.0%, respectively. At the same mass concentration of NPs, the HTC showed a variable behaviour with the effective TC of NFs.

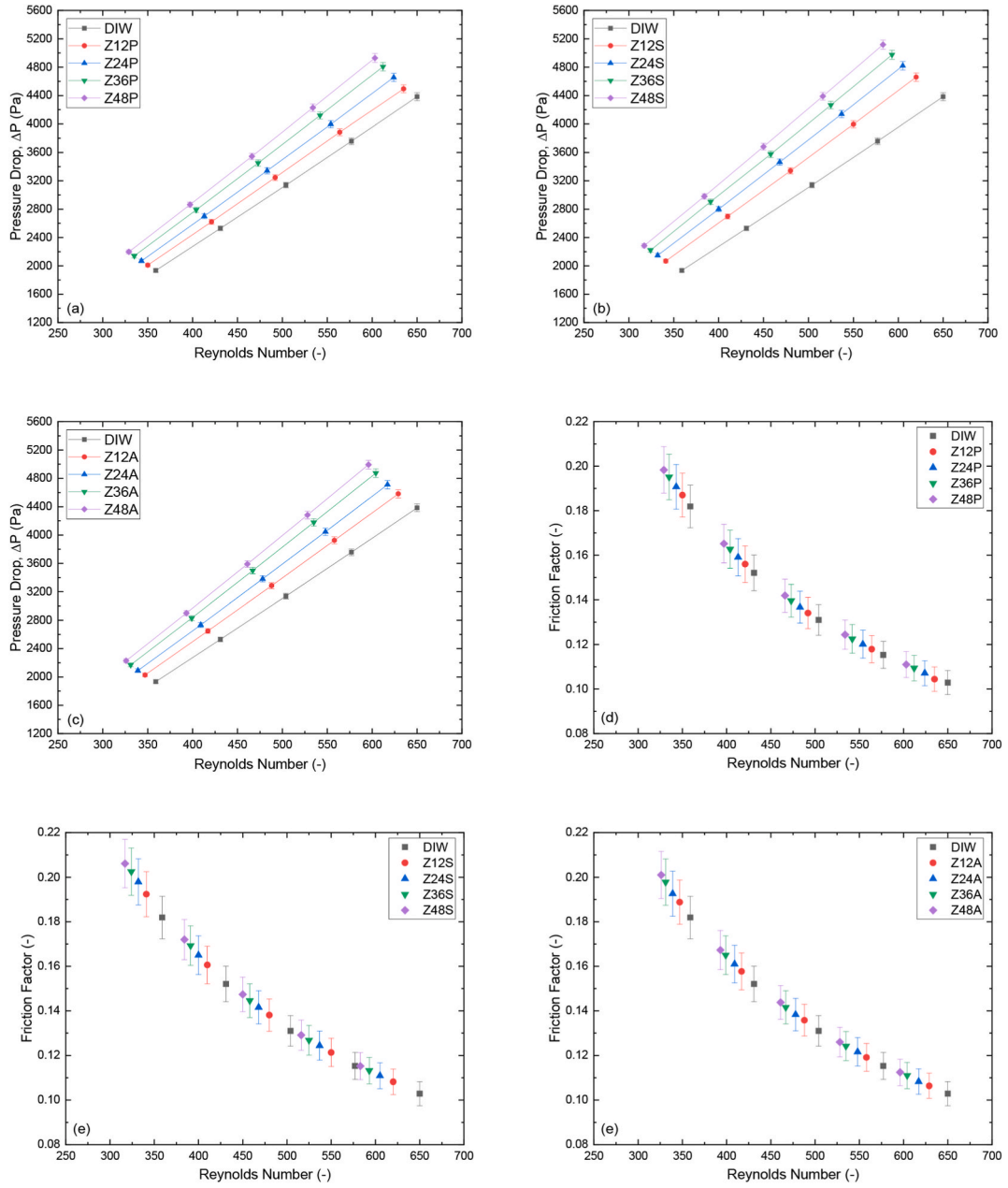

Fig. 10. Comparison of Pressure Drop and Friction Factor across the flow channel at different Reynolds Numbers (a) DIW NFs (b) SHMP NFs (c) ACAC NFs (d) DIW NFs (e) SHMP NFs (f) ACAC NFs.

4. The Nusselt number strongly depends upon the HTC and the TC of the NFs. Hence, it possessed an increasing behaviour with the rise in HTC and an opposite trend with the TC of the NFs. For Pure and SHMP-based NFs, the Nusselt number decreased due to the dominancy of NFs' TC. In contrast, for ACAC-based NFs, the Nusselt number increased due to the dominant effect of convective HTC.
5. The pressure gradient of NFs showed a strong dependency on the rise in NP's mass concentration and the fluid flow rate, possibly due to a rise in the VC of NFs. The maximum pressure gradient recorded across the minichannel test section for Pure, SHMP, and ACAC-based NFs was 12.0%, 16.0%, and 13.0%, respectively.
6. The friction factor recorded across the test setup was directly dependent on the loading of the ZnO NPs. The maximum friction factor losses across the test section for Pure, SHMP, and ACAC-based NFs were 7.0%, 12.0%, and 9.0%, respectively.

The current study revealed the potential of the investigated ZnO NFs for present and future heat transfer applications with and without stabilising agents. In future studies, the NFs with comparatively higher TC and lower VC may be explored at ultra-low

temperatures rather than above ambient to evaluate their potential for refrigeration and air conditioning applications. Furthermore, new techniques to mitigate the high production cost of the NPs should be explored, focusing on non-corrosive NPs for the extended life of the thermal and heat transfer systems. Finally, the solution to the subject-cited problems will lead to the industrial applications of the NFs.

Author statement

Adnan Qamar: Conceptualization. Rabia Shaukat: Conceptualization. Shahid Imran: Methodology, testing. Muhammad Farooq: Methodology, testing. Muhammad Amjad: Data processing. Zahid Anwar: Data processing. Hassan Ali: Data processing. Muhammad Farhan: Validation, drafting. M.A. Mujtaba: Validation, drafting. Theodosios Korakianitis: Validation, drafting. M.A. Kalam: Formal analysis and discussion. Fares Almomani: Formal analysis and discussion, Writing - Original Draft, editing. M.A. Mujtaba: Visualization, editing. Fares Almomani: Visualization, editing.

Declaration of competing interest

The authors declare that they have no known competing financial interests or personal relationships that could have appeared to influence the work reported in this paper.

Data availability

Data will be made available on request.

Acknowledgement

The authors of the present investigation would like to pay their sincere gratitude to the University of Engineering and Technology (UET), Lahore, Pakistan, for providing funding and access to the scientific instruments for the execution of the present research investigation under Research Grant No. ORIC/105-ASRB/3084, ORIC/101-ASRB/4452 and ORIC/101-ASRB/4453. Open Access funding provided by the Qatar National Library.

References

[1] G. Colangelo, E. Favale, M. Milanese, A. de Risi, D. Laforgia, Cooling of electronic devices: nanofluids contribution, Appl. Therm. Eng. 127 (2017) 421–435, https://doi.org/10.1016/j.applthermaleng.2017.08.042.
[2] M.U. Sajid, H.M. Ali, Recent advances in application of nanofluids in heat transfer devices: a critical review, Renew. Sustain. Energy Rev. 103 (2019) 556–592, https://doi.org/10.1016/j.rser.2018.12.057.
[3] S.M. Sohel Murshed, C.A. Nieto de Castro, A critical review of traditional and emerging techniques and fluids for electronics cooling, Renew. Sustain. Energy Rev. 78 (2017) 821–833, https://doi.org/10.1016/j.rser.2017.04.112.
[4] H. M. Maghrabie et al., "Intensification of heat exchanger performance utilizing nanofluids," Int. J. Thermofluids, vol. 10, 2021, doi: 10.1016/j.ijft.2021.100071.
[5] T. P. Das, Sarit K., Stephen U. S. Choi, Wenhua Yu, *Nanofluids Science And Technology*.
[6] A. Jafarimoghaddam, S. Aberoumand, K. Javaherdeh, A.A.A. Arani, R. Jafarimoghaddam, Al/oil nanofluids inside annular tube: an experimental study on convective heat transfer and pressure drop, Heat Mass Tran. 54 (4) (2018) 1053–1067, https://doi.org/10.1007/s00231-017-2199-9.
[7] K.N. Ramesh, T.K. Sharma, G.A.P. Rao, Latest advancements in heat transfer enhancement in the micro-channel heat sinks: a review, Springer Netherlands 28 (4) (2021), https://doi.org/10.1007/s11831-020-09495-1.
[8] K.R. Aglawe, R.K. Yadav, S.B. Thool, Preparation, applications and challenges of nanofluids in electronic cooling: a systematic review, Mater. Today Proc. 43 (2020) 366–372, https://doi.org/10.1016/j.matpr.2020.11.679.
[9] A. Qamar, et al., Preparation and dispersion stability of aqueous metal oxide nanofluids for potential heat transfer applications: a review of experimental studies, J. Therm. Anal. Calorim. 147 (1) (2022) 23–46, https://doi.org/10.1007/s10973-020-10372-z.
[10] S. Chakraborty and P. K. Panigrahi, "Stability of nanofluid: a review," Appl. Therm. Eng., vol. 174, 2020, doi: 10.1016/j.applthermaleng.2020.115259.
[11] K.S. Suganthi, K.S. Rajan, Temperature induced changes in ZnO-water nanofluid: zeta potential, size distribution and viscosity profiles, Int. J. Heat Mass Tran. 55 (2012) 7969–7980, https://doi.org/10.1016/j.ijheatmasstransfer.2012.08.032.
[12] R.N. Radkar, B.A. Bhanvase, D.P. Barai, S.H. Sonawane, Intensified convective heat transfer using ZnO nanofluids in heat exchanger with helical coiled geometry at constant wall temperature, Mater. Sci. Energy Technol. 2 (2) (2019) 161–170, https://doi.org/10.1016/j.mset.2019.01.007.
[13] I.M. Shahrul, I.M. Mahbubul, R. Saidur, M.F.M. Sabri, Experimental investigation on Al2O3-W, SiO2-W and ZnO-W nanofluids and their application in a shell and tube heat exchanger, Int. J. Heat Mass Tran. 97 (2016) 547–558, https://doi.org/10.1016/j.ijheatmasstransfer.2016.02.016.
[14] M. Adil, H.M. Zaid, L.K. Chuan, N.R.A. Latiff, Effect of dispersion stability on electrorheology of water-based ZnO nanofluids, Energy Fuel. 30 (7) (2016) 6169–6177, https://doi.org/10.1021/acs.energyfuels.6b01116.
[15] S. Ponmani, J. Karen, M. William, R. Samuel, R. Nagarajan, J.S. Sangwai, Formation and characterization of thermal and electrical properties of CuO and ZnO nanofluids in xanthan gum, Colloids Surfaces A Physicochem. Eng. Asp. 443 (2014) 37–43, https://doi.org/10.1016/j.colsurfa.2013.10.048.
[16] T. Elango, A. Kannan, K.K. Murugavel, Performance study on single basin single slope solar still with different water nano fluids, Desalination 360 (2015) 45–51, https://doi.org/10.1016/j.desal.2015.01.004.
[17] W.H. Azmi, K. V Sharma, R. Mamat, G. Naja, M.S. Mohamad, The enhancement of effective thermal conductivity and effective dynamic viscosity of nanofluids-A review, Renew. Sustain. Energy Rev. 53 (2016) 1046–1058, https://doi.org/10.1016/j.rser.2015.09.081.
[18] A. Einstein, A new determination of molecular dimensions, Ann. Phys. 19 (1906) 289–306 [Online]. Available: https://ci.nii.ac.jp/naid/10015778632/en/.
[19] S.M.S. Murshed, P. Estellé, A state of the art review on viscosity of nanofluids, Renew. Sustain. Energy Rev. 76 (2017) 1134–1152, https://doi.org/10.1016/j.rser.2017.03.113.
[20] S. Aberoumand, et al., Thermo-electro-rheological behaviour of vanadium electrolyte-based electrochemical graphene oxide nanofluid designed for redox flow battery, J. Mol. Liq. 338 (2021), 116860, https://doi.org/10.1016/j.molliq.2021.116860.
[21] A. Jafarimoghaddam, H. Aberoumand, S. Aberoumand, A.A.A. Arani, A. Habibollahzade, MHD wedge flow of nanofluids with an analytic solution to an especial case by Lambert W-function and Homotopy Perturbation Method, Eng. Sci. Technol. an Int. J. 20 (6) (2017) 1515–1530, https://doi.org/10.1016/j.jestch.2017.11.002.

[22] A. Qamar, et al., Dispersion stability and rheological characteristics of water and ethylene glycol based ZnO nanofluids, Therm. Sci. 25 (3) (2021) 1989–2001, https://doi.org/10.2298/TSCI200110187Q.
[23] S. Nabati Shoghl, J. Jamali, M. Keshavarz Moraveji, Electrical conductivity, viscosity, and density of different nanofluids: an experimental study, Exp. Therm. Fluid Sci. 74 (2016) 339–346, https://doi.org/10.1016/j.expthermflusci.2016.01.004.
[24] D. Branch, Y.R. Club, D. Branch, Experimental study on turbulent heat transfer, pressure drop, and thermal performance of ZnO/water nanofluid flow in a circular tube, Therm. Sci. 18 (2014) 1315–1326, https://doi.org/10.2298/TSCI131114022S.
[25] A. Topuz, T. Engin, A. Alper Özalp, B. Erdoğan, S. Mert, A. Yeter, Experimental investigation of optimum thermal performance and pressure drop of water-based Al2O3, TiO2 and ZnO nanofluids flowing inside a circular microchannel, J. Therm. Anal. Calorim. 131 (2018) 2843–2863, https://doi.org/10.1007/s10973-017-6790-6.
[26] A.H. Rasheed, H.B. Alias, S.D. Salman, Experimental and numerical investigations of heat transfer enhancement in shell and helically microtube heat exchanger using nanofluids, Int. J. Therm. Sci. 159 (2021), 106547, https://doi.org/10.1016/j.ijthermalsci.2020.106547.
[27] J. Jeong, C. Li, Y. Kwon, J. Lee, S. Hyung, R. Yun, Particle shape effect on the viscosity and thermal conductivity of ZnO nanofluids, Int. J. Refrig. 36 (8) (2013) 2233–2241, https://doi.org/10.1016/j.ijrefrig.2013.07.024.
[28] S. Aberoumand, A. Jafarimoghaddam, M. Moravej, H. Aberoumand, K. Javaherdeh, Experimental study on the rheological behavior of silver-heat transfer oil nanofluid and suggesting two empirical based correlations for thermal conductivity and viscosity of oil based nanofluids, Appl. Therm. Eng. 101 (2016) 362–372, https://doi.org/10.1016/j.applthermaleng.2016.01.148.
[29] S.H. Kim, S.R. Choi, D. Kim, Thermal conductivity of metal-oxide nanofluids: particle size dependence and effect of laser irradiation, J. Heat Tran. 129 (3) (2007) 298–307.
[30] M. Sharifpur, S.O. Giwa, K.Y. Lee, H. Ghodsinezhad, J.P. Meyer, Experimental investigation into natural convection of zinc oxide/water nanofluids in a square cavity, 0, Heat Tran. Eng. (2020) 1–13, https://doi.org/10.1080/01457632.2020.1818384, 0.
[31] A.H. Meghdadi Isfahani, M. Afrand, Experiment and Lattice Boltzmann numerical study on nanofluids flow in a micromodel as porous medium, Phys. E Low-Dimensional Syst. Nanostructures 94 (June) (2017) 15–21, https://doi.org/10.1016/j.physe.2017.07.008.
[32] M. Niknejadi, M. Afrand, A. Karimipour, A. Shahsavar, A.H. Meghdadi Isfahani, Experimental investigation of the hydrothermal aspects of water-Fe3O4 nanofluid inside a twisted tube, J. Therm. Anal. Calorim. 143 (1) (2021) 801–810, https://doi.org/10.1007/s10973-020-09271-0.
[33] K.G. Dehkordi, A. Karimipour, M. Afrand, D. Toghraie, A.H.M. Isfahani, Molecular dynamics simulation concerning nanofluid boiling phenomenon affected by the external electric field: effects of number of nanoparticles through Pt, Fe, and Au microchannels, J. Mol. Liq. 324 (2021), 114775, https://doi.org/10.1016/j.molliq.2020.114775.
[34] S. Karimi, M.M. Heyhat, A.H.M. Isfahani, A. Hosseinian, Experimental investigation of convective heat transfer and pressure drop of SiC/water nanofluid in a shell and tube heat exchanger, Heat Mass Transf. und Stoffuebertragung 56 (8) (2020) 2325–2331, https://doi.org/10.1007/s00231-020-02844-7.
[35] H. Azimy, A.H. Meghdadi Isfahani, M. Farahnakian, Investigation of the effect of ultrasonic waves on heat transfer and nanofluid stability of MWCNTs in sono heat exchanger: an experimental study, Heat Mass Transf. und Stoffuebertragung 58 (3) (2022) 467–479, https://doi.org/10.1007/s00231-021-03126-6.
[36] H. Siddiqi, et al., Heat transfer and pressure drop characteristics of ZnO/DIW based nanofluids in small diameter compact channels : an experimental study, Case Stud. Therm. Eng. 39 (September) (2022), 102441, https://doi.org/10.1016/j.csite.2022.102441.
[37] S. Ferrouillat, A. Bontemps, O. Poncelet, O. Soriano, J.A. Gruss, Influence of nanoparticle shape factor on convective heat transfer and energetic performance of water-based SiO2 and ZnO nanofluids, Appl. Therm. Eng. 51 (2013) 839–851, https://doi.org/10.1016/j.applthermaleng.2012.10.020.
[38] A. Abdollahi, H.A. Mohammed, S.M. Vanaki, A. Osia, M.R. Golbahar Haghighi, Fluid flow and heat transfer of nanofluids in microchannel heat sink with V-type inlet/outlet arrangement, Alex. Eng. J. 56 (2017) 161–170, https://doi.org/10.1016/j.aej.2016.09.019.
[39] R. Ramirez-Tijerina, C.I. Rivera-Solorio, J. Singh, K.D.P. Nigam, Numerical study of heat transfer enhancement for laminar nanofluids flow, Appl. Sci. (12) (2018) 1–18, https://doi.org/10.3390/app8122661.
[40] T.T. Loong, H. Salleh, A. Khalid, H. Koten, Thermal performance evaluation for different type of metal oxide water based nanofluids, Case Stud. Therm. Eng. 27 (July) (2021), 101288, https://doi.org/10.1016/j.csite.2021.101288.
[41] N.A.C. Sidik, H.A. Mohammed, O.A. Alawi, S. Samion, A review on preparation methods and challenges of nanofluids, Int. Commun. Heat Mass Tran. 54 (2014) 115–125, https://doi.org/10.1016/j.icheatmasstransfer.2014.03.002.
[42] A. Qamar, Z. Anwar, H. Ali, S. Imran, R. Shaukat, M. Mujtaba Abbas, Experimental investigation of dispersion stability and thermophysical properties of ZnO/DIW nanofluids for heat transfer applications, Alex. Eng. J. (2021), https://doi.org/10.1016/j.aej.2021.09.028.
[43] V.R. Venu Gopal, S. Kamila, Effect of temperature on the morphology of ZnO nanoparticles: a comparative study, Appl. Nanosci. 7 (3–4) (2017) 75–82, https://doi.org/10.1007/s13204-017-0553-3.
[44] D. Cabaleiro, L. Colla, F. Agresti, L. Lugo, L. Fedele, Transport properties and heat transfer coefficients of ZnO/(ethylene glycol + water) nanofluids, Int. J. Heat Mass Tran. 89 (2015) 433–443, https://doi.org/10.1016/j.ijheatmasstransfer.2015.05.067.
[45] I.M. Mahbubul, R. Saidur, M.A. Amalina, Latest developments on the viscosity of nanofluids, Int. J. Heat Mass Tran. 55 (4) (2012) 874–885, https://doi.org/10.1016/j.ijheatmasstransfer.2011.10.021.
[46] A. Jafarimoghaddam, S. Aberoumand, Exact approximations for skin friction coefficient and convective heat transfer coefficient for a class of power law fluids flow over a semi-infinite plate: results from similarity solutions, Eng. Sci. Technol. an Int. J. 20 (3) (2017) 1115–1121, https://doi.org/10.1016/j.jestch.2016.10.020.
[47] B.C. Pak, Y.I. Cho, Hydrodynamic and heat transfer study of dispersed fluids with submicron metallic oxide particles, Exp. Heat Tran. 11 (2) (1998) 151–170, https://doi.org/10.1080/08916159808946559.
[48] W.R. Yimin Xuana, Conceptions for heat transfer correlation of nanofluids, Int. J. Heat Mass Tran. 43 (2000) 3701–3707.
[49] R.K. Shah, Thermal entry length solutions for the circular tube and parallel plates, Proceedings of 3rd national heat and mass transfer conference 1 (1975) 11–75.
[50] F.P. Incropera, T.L. Bergman, A.S. Lavine, D.P. DeWitt, Fundamentals of Heat and Mass Transfer, 2011, https://doi.org/10.1073/pnas.0703993104.
[51] R.J. Moffat, Describing the uncertainties in experimental results, Exp. Therm. Fluid Sci. 1 (1) (1988) 3–17, https://doi.org/10.1016/0894-1777(88)90043-X.
[52] P.C. Mishra, S. Mukherjee, S.K. Nayak, A. Panda, A brief review on viscosity of nanofluids, Int. Nano Lett. 4 (4) (2014) 109–120, https://doi.org/10.1007/s40089-014-0126-3.
[53] R. Prasher, P. Bhattacharya, P.E. Phelan, Thermal conductivity of nanoscale colloidal solutions (nanofluids), Phys. Rev. Lett. 94 (2) (2005) 3–6, https://doi.org/10.1103/PhysRevLett.94.025901.
[54] S. Mukherjee, P.C. Mishra, S.K.S. Parashar, P. Chaudhuri, Role of temperature on thermal conductivity of nanofluids: a brief literature review, Heat Mass Transf. und Stoffuebertragung 52 (2016) 2575–2585, https://doi.org/10.1007/s00231-016-1753-1.